Excerpt from the Proceedings of the COMSOL Conference 2010 Paris

A Study of Distributed Feed-Back Fiber Laser Sensor for Aeronautical Applications Using COMSOL Multiphysics

I. Lancranjan*[1], C. Gavrila[2], Sorin Miclos[3], Dan Savastru[3],
[1] Advanced Study Centre - National Institute for Aerospace Research “Elie Carafoli”, Bucharest, Romania, [2] Technical University of Civil Engineering Bucharest, Romania, [3] National Institute R&D of Optoelectronics, INOE 2000, Bucharest, Romania
*Corresponding author: postal address: 220, Iuliu Maniu Blvd, Sector 6, 061126 Bucharest, Romania, email address: J_J_F_L@yahoo.com

Abstract: Distributed Feedback Fiber Laser (DFB-FL) sensors are increasingly used in aeronautical applications. One of the newest such application consists in detecting the “transition” zone between laminar and turbulent air flow upon the extrados surface of an aircraft wing. In this specific application DFB-FL are operated as air pressure sensors monitoring amplitude variations of ~1 Pa (laminar flow) up to ~10Pa (turbulent flow) with repetition frequencies in the range 500 Hz – 10kHz. DFB-FL sensors consist in single mode rare earth ions doped optic fiber in which Bragg grating are created by using UV radiation. In most cases, as laser active centers, Er^{3+} ions are used for doping the optic fiber. DFB-FL use as extremely sensitive sensors relies on laser resonator parameter variation induced by the environment factor. Among the laser resonator parameter variation the modification Bragg grating wavelength and laser power optic fiber transmission are included. In this paper, we propose a study of an Er^{3+} DFB-FL sensor using COMSOL Multiphysics. The main purpose of this study is to provide essential data for a proper design of a device of this type.

Keywords: DFB-FL sensor, laminar and turbulent flow

1. Introduction

This paper presents preliminary theoretical analysis results obtained in investigating distributed feedback fiber lasers (DFB-FL) and distributed Bragg reflector fiber lasers (DBR-FL) dedicated to a new aeronautical application consisting into detection of transition zone existing between the laminar and turbulent air flow upon the extrados wing surface of an aircraft. DFB-FL and DBR-FL possess certain unique properties that make them quite attractive for a number of different applications. They are inherently fiber compatible, and very simple passive thermal stabilization is sufficient to ensure the stability of the laser.

A number of different active dopants such as erbium, ytterbium, neodymium and thulium can be used in order to cover different windows of the optical spectrum. These features, combined with the ability to define the emitted wavelength precisely through the grating structure along with the narrow linewidth and low relative intensity noise (RIN), make DFB-FL and DBR-FL very advantageous for telecommunication applications [1]–[3]. In addition, a number of DFB fiber lasers can be configured in a parallel array to provide flexibility in pumping conditions and provide pump redundancy [2], [4].

Robust single polarization and narrow linewidth of DFB lasers are very desirable for sensor systems [5]–[7]. Alternatively, DFB lasers can be made to operate in stable dual polarization regime so that simultaneous measurements can be carried out [8]–[10]. In addition to the sensing and telecom applications, DFB fiber lasers suitable for high-power applications have been demonstrated [11].

2. Theory

An important aeronautical application of fiber optic sensors consists in determination of *transition zone* between *laminar* and *turbulent flow* of air along the wing surface. Intermittent regime occurring in-between these two regions (transition) is characterized by turbulent bursts in laminar flow.

The basic idea of this type of measurement is to evaluate the pressure variation in the two zones:

1. Laminar flow - relative constant value of air static pressure, low frequency (~ 100 Hz) and small amplitude (ΔP ~ 1 Pa) pressure variations.

2. Turbulent flow - larger and nonstationary value of air static pressure, higher frequency (~ 10 kHz) and higher amplitude (ΔP ~ 10 Pa) pressure variations.

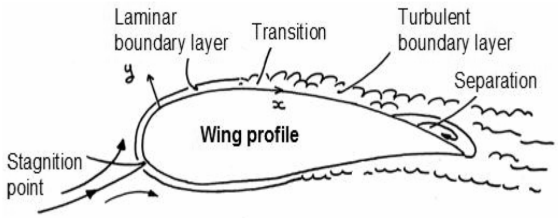

Fig. 1 Schematic representation of the investigated aeronautical application of DFB-FL and DBR-FL.

The main investigated aeronautical DFB-FL and DBR-FL sensors application consists in determination of the transition zone (line) between laminar and turbulent air flow along the aircraft wing surface. The laminar and turbulent boundary layers can be observed in Fig. 1.

Possible fiber optic "reaction": linear glass strain deformation (glass Young's modulus of elasticity is $E = 50 \div 90 \cdot 10^9$ N/m^2) under air turbulent pressure bursts (deformations of $10^{-9} \div 10^{-8}$ m) is extremely difficult to measure even by optical interferometer methods. In this situation micro-bending of fiber optic appears to be more feasible deformation as an effect of turbulent air flow pressure bumps. The laminar and turbulent air flow zones along the aircraft wing surface are indicated. One possible position of the fiber optic sensor can be observed.

In Fig. 2 it can be observed that the fiber optic sensor is embedded close (0.2 mm depth) to the wing surface. The fiber optic sensor is placed into a soft material, like paraffin, under an 0.2 mm thick aluminum foil.

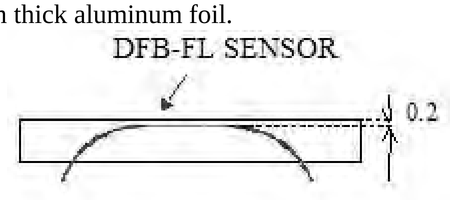

Fig.2 Insights of one possible way of mounting the DFB-FL and/or DBR-FL in the wing for determination of transition zone between laminar and turbulent air flow along the aircraft wing surface

One possible procedure for reading the fiber optic sensor is presented schematically in Fig. 3. This possible procedure is based on precise evaluation of lasing wavelength, lasing, which depends on the laser resonant cavity length.

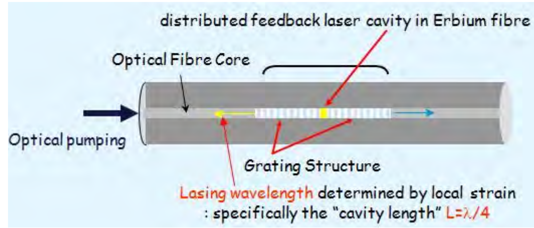

Fig. 3 Some insights about the structure of the DFB-FL and/or DBR-FL proposed to be used for the determination of the transition zone between laminar and turbulent air flow along the wing surface

Traditionally, there have been three main DFB laser cavity designs that offer different performance and distinctive operational characteristics, presented in the followings.

It was recently shown that the classic parametric optimization approach for a DFB laser, i.e., the definition of the optimum resonator geometry and dimensional values, is analogous to Rigrod optimization [18] of reflectivity in Fabry–Pérot laser cavities of fixed length. It can also be shown that it is possible to further improve the DFB laser efficiency by increasing the effective cavity length without changing the total device length and optimum reflectivity, using a step-apodized profile. Both optimization approaches are parametric in nature. The main cavity features are defined a priori, and their parameters are continuously varied until a maximum efficiency is reached. However, none of these approaches guarantees that the ultimate, i.e., maximum possible, efficiency for the given medium has been achieved. In this paper, a drastically different approach is followed.

Using this information, the developed algorithm calculates the required grating strength distribution that results in the desired optimum signal, pump, and gain distribution.

In Fig. 4, 5 and 6 the schematics of the investigated DFB-FL structures are presented. The main effort pointed on structures presented in Fig. 5 and 6.

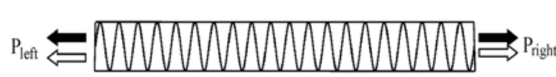

Fig. 4 Refractive index profile for conventional DFB laser designs. The classic design and two-wavelength bidirectional operation

The classic design and two-wavelength bidirectional operation is displayed in Fig. 4. It consists of a uniform refractive index grating, with constant amplitude and constant period, incorporated in an active medium. This type of DFB laser operates at two fundamental longitudinal modes at different wavelengths, corresponding to the edges of the grating bandgap, and gives symmetric output powers from both ends, which are equally divided between these two modes [12]. Such a cavity provides dual-wavelength bidirectional operation.

Fig. 5 Refractive index profile for conventional DFB laser designs. Symmetric-phase shifted design and single-wavelength bidirectional operation

Fig. 5 shows the symmetric-phase shifted design and single-wavelength bidirectional operation. In practice, however, single-wavelength operation is desirable. This is achieved by introducing a π–shift in the spatial phase of the grating [13]–[15]. If the phase shift is located in the middle of the grating due to the symmetry of the cavity, the output powers at both ends are equal. Such a cavity provides single-wavelength operation, coinciding with the grating Bragg wavelength, and bidirectional operation.

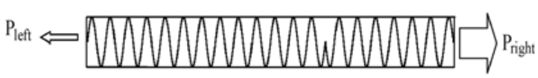

Fig. 6 Refractive index profile for conventional DFB laser designs. Asymmetric π-phase-shifted design and single-wavelength unidirectional operation

Asymmetric π-phase-shifted design and single-wavelength unidirectional operation is shown in Fig. 6. In addition to single-wavelength emission, unidirectional is a very desirable feature of high-performance lasers. By placing the phase shift asymmetrically with respect to the grating center, as shown in Fig. 6, larger output power is obtained from the shorter end [10], [16]. In this asymmetric design, the maximum output power from the desired end is obtained for a particular phase-shift position and coupling coefficient value.

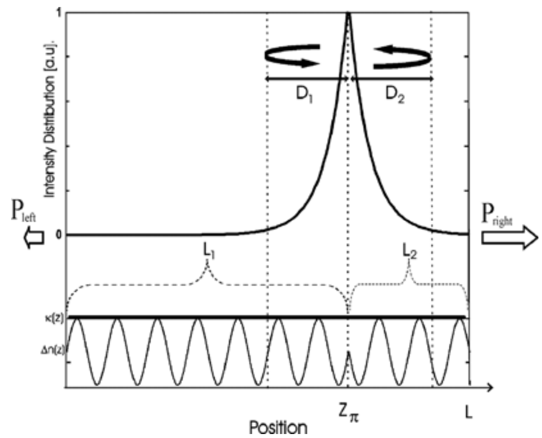

Fig. 7 Standard asymmetric DFB-FL structure

Standard asymmetric DFB-FL structure is illustrated in Fig. 7. The optimum position of the π-phase shift position (z_p) can be observed. D_1 and D_2 represent the "penetration" depth of electromagnetic field into the Bragg grating zones.

The standard coupled-mode equations for counter-propagating fields are used (see, e.g., [20]). The electric field (E) is the sum of two counter-propagating fields (*A* and *B*):

$$\frac{dA(z)}{dz} = \alpha(z)A(z) + \kappa(z)B(z)e^{i\Gamma(z)} \qquad (1)$$

$$\frac{dB(z)}{dz} = -\alpha(z)B(z) + \kappa(z)A(z)e^{-i\Gamma(z)} \qquad (2)$$

(2)

where *A(z)* is the amplitude of the forward-propagating field, *B(z)* is the amplitude of the backward-propagating field, $A(z)e^{-i\Gamma(z)}$ represents the envelope of the forward-propagating field, $B(z)e^{i\Gamma(z)}$ represents the envelope of the backward-propagating field, α(z) is the field gain, $\kappa(z)$ is the coupling coefficient while Γ (z) is the spatial phase factor or coefficient. A schematic representation of coupled-mode procedure or method, used for numerical evaluation of DFB-FL structure is presented in Fig. 8.

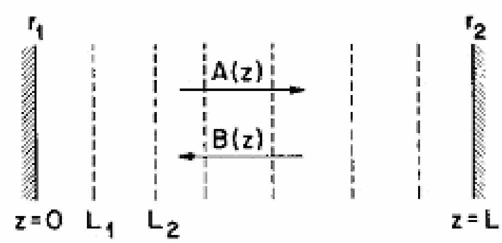

Fig. 8 Schematic representation of coupled-mode procedure/method

Designating by α (z) the net field gain including the background loss and ϕ (z) the Bragg grating phase, the spatial phase factor/coefficient Γ (z) will be given by this equation, where β is the unperturbed waveguide mode:

$$\Gamma(z) = 2\beta(z) - \phi(z) \tag{3}$$

The equation defining the Bragg grating phase ϕ (z) is:

$$\phi(z) = \int_0^z \frac{2\pi}{\Lambda(z^*)} dz^* \tag{4}$$

where Λ (z) represents the local grating period. The average signal intensity definition is:

$$S(z) = A^2(z) + B^2(z) \tag{5}$$

While the definition of the intensity difference between the counter-propagating fields is:

$$D(z) = A^2(z) - B^2(z) \tag{6}$$

The intensity difference D(z) can be expressed as:

$$D(z) = D(0) + 2\int_0^z \alpha(z^*) \cdot S(z^*) dz^* \tag{7}$$

The standard coupled-mode propagation equations for counter-propagating fields are can be manipulated to provide expressions for *k(z)*, the coupling coefficient of the electromagnetic field:

$$k(z) = \frac{\dfrac{dS(z)}{2z} - D(z)\alpha(z)}{\cos(\Gamma(z))\sqrt{S^2(z) - D^2(z)}} \tag{8}$$

The usual DFB laser boundary conditions are:

$$A(0) = B(L) = 0 \tag{9}$$

The new/transformed DFB laser boundary conditions are:

$$\begin{aligned} D(0) &= -B^2(0) = 0 \\ D(L) &= A^2(L) = S(L) \end{aligned} \tag{10}$$

These boundary conditions represent the basis of our design method. Given S(z), α(z) and Λ(z), we can use them to find D(z) and then the required coupling coefficient distribution can be calculated:

$$n(z) = n_0 + \Delta n(z) \cdot \cos(\phi(z)) \tag{11}$$

The coupling coefficient defines the amount of the periodic perturbation required. If this perturbation is sinusoidal the varying refractive-index modulation in the form is defined by the above equation. n_0 is the effective refractive index and Δn is the modulation amplitude.

The reflection coefficient of a grating with constant gain at the Bragg wavelength is:

$$r = \frac{-\kappa \cdot \sinh(\gamma L)}{\gamma \cdot \cosh(\gamma L) - \alpha \cdot \sinh(\gamma L)} \tag{12}$$

Here γ coefficient is $\gamma = \sqrt{\kappa^2 + \alpha^2}$.

The approximation of reflection coefficient of a grating with constant gain at the Bragg wavelength is given by $r \approx -\tanh(\kappa L)$.

The necessary condition for the validation of the above equation is $\alpha \ll \kappa$.

The reflectivity of the Bragg grating is equal to the reflectivity of a passive grating with no gain:

$$R = r^2 \approx \tanh^2(\kappa L) \tag{13}$$

Due to the distributed nature of the reflection process in gratings, the incident wave penetrates into the grating before reemerging at the front end. It refers to the case of the case of constant gain and at the Bragg wavelength:

$$D = \frac{1}{2} \cdot \frac{\alpha L\left(\dfrac{\tanh(\gamma L)}{\gamma L} - \dfrac{1}{\cosh^2(\gamma L)}\right) + \tanh^2(\gamma L)}{\alpha \cdot \tanh^2(\gamma L) + \gamma \cdot \tanh(\gamma L)} \tag{14}$$

In the case of a phase-shifted DFB laser, the total length of effective cavity in which the fields are circulating is:

$$L_{eff} = D_1 + D_2 \approx \left(\frac{|r_1|}{2\kappa_1} + \frac{r_2}{2\kappa_2}\right) \tag{15}$$

D_1 and D_2 are the penetration depths into the Bragg grating segments on the left-hand side and on the right-hand side of the phase shift, respectively. In the case of a uniform refractive index profile, the coupling coefficient is constant.

A mode propagating on a straight fiber or waveguide fabricated from non-absorbing, non-scattering materials will in principle propagate indefinitely without any loss of power. However, if a bend is introduced, the translational invariance is broken and power is lost from the mode as it propagates into, along and out of the bend. This applies to the fundamental mode in the case of single-mode fibers.

Two types of optic fiber bend losses can be considered [20 - 22]:

- Transition loss is associated with the abrupt or rapid change in curvature at the beginning and the end of a bend;
- Pure bend loss is associated with the loss from the bend of constant curvature in between the optic fiber.

The transition loss can be described by an abrupt change in the curvature k from the straight waveguide (k ~ 0) to that of the bent waveguide of constant radius R_b ($k = 1/R_b$). The fundamental-mode field is shifted slightly outwards in the plane of the bend, thereby causing a miss-match with the field of the straight waveguide, as presented in Fig. 9.

The fractional loss in fundamental-mode power, $\delta P/P$, can be calculated from the overlap integral between the fields. Within the Gaussian approximation to the fundamental mode field and assuming that the spot size s and core radius or half-width ρ are approximately equal, where V is the fiber or waveguide parameter and D is the relative index difference this gives:

$$\frac{\delta P}{P} \approx \frac{1}{16} \cdot \frac{V^4}{\Delta^2} \cdot \frac{\rho^2}{R_b^2} \tag{16}$$

Minimizing transition loss can be achieved by considering a number of techniques for significantly reducing transition loss. In Fig. 9 this can be seen as being equivalent to displacing the bent core downwards so that the two fundamental-mode fields overlap. Alternatively, if a gradual increase in curvature is introduced between the straight and uniformly bent sections, the fundamental field of the straight waveguide will evolve approximately adiabatically into the offset field of the uniformly bent section.

The pure bent loss is defined by the fundamental mode continuously optical power loses when propagating along the curved path of the core of constant radius R_b. It is assumed that the cladding is essentially unbounded and not affected by the fiber optic bent, keeping a constant cladding refractive index value, n_{cl}. The radiation loss increases rapidly with decreasing bend radius and occurs predominantly in the plane of the bend; in any other plane the effective bend radius is larger and hence the loss is very much reduced, as presented in Fig. 10.

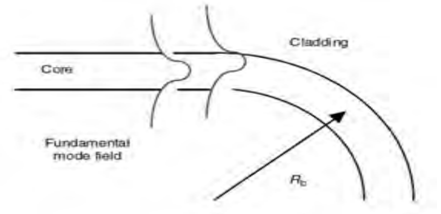

Fig. 9 Outward shift in the fundamental-mode electric field on entering a bend

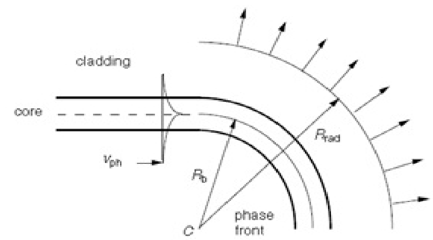

Fig. 10 Schematic of the bending effect of a fiber laser

It has to be observed that the phase velocity any where on the modal phase front rotating around the bend cannot exceed the speed of light in the cladding. Hence, beyond radius R_{rad} the modal field must necessarily radiate into the cladding, the radiation being emitted tangentially. The interface between the guided portion of the modal field around the bend and the radiated portion at R_{rad} is known as the radiation caustic, and it is the apparent origin of radiation. R_{rad} can be defined by the equation:

$$R_{rad} = \frac{C}{\Omega \cdot n_{cl}} \tag{17}$$

The present theoretical analysis is developed by considering step-index optical fibers (with a step profile of the refractive index). In terms of the core and cladding modal parameters U and W, respectively, relative index difference Δ, core radius ρ, fiber parameter V and the bending radius R_b, an approximate expression for γ for the fundamental mode of a step-index fiber has the form [20 - 22]:

$$\gamma = \sqrt{\frac{\pi\rho}{R_b}} \frac{V^2\sqrt{W}}{2\rho U^2} \exp\left(-\frac{4}{3}\Delta \frac{R_b}{\rho}\frac{W^3}{V^2}\right) \tag{18}$$

where R_b is necessarily large compared to ρ because it is not possible to bend a fiber into a radius much below 10 mm without breakage. The pure bend loss coefficient is most sensitive to the expression inside the exponent because R_b and ρ. Loss decreases very rapidly with increasing values of R_b or Δ or V (since W also increases with V), and becomes arbitrarily small as R_b tends to infinity.

6. Numerical Simulation Results

Two numerical simulation procedures were used:

- one relaying on SCILAB software package, based on the above mentioned equations;

•the second one relaying on COMSOL software packages.

Numerical simulations were performed for optical fiber with and without doping with erbium ions (Er^{3+}). No significant differences were observed for doped or undoped optical fibers. The numerical simulations were performed using 1.550 µm as the laser wavelength.

In the first stage, transition loss was simulated. Using (16) relative input power variation was calculated as:

$$P_{rel} = \frac{V^4}{16 \cdot \Delta^2} \cdot \frac{\rho^2}{R_b^2} \quad (19)$$

where ρ = 5 µm is the core radius, R_b = 5 mm is the radius of curvature, while Δ – relative index difference and V – modal parameter are calculated as it follows:

$$\Delta = \frac{n_{core}^2 - n_{clad}^2}{n_{core}^2} \quad (20)$$

$$V = \frac{2\pi \cdot \rho}{\lambda} \sqrt{n_{core}^2 - n_{clad}^2} \quad (21)$$

n_{core} = 1.4457 is the refractive index of the core, with a diameter of 10 µm, n_{clad} = 1.4378 is the refractive index of the cladding with an external diameter of 80 µm, while λ = 1.55 µm denotes the wavelength. Fig. 16 illustrates the variation of relative input power P_{rel} vs. radius of curvature R_b.

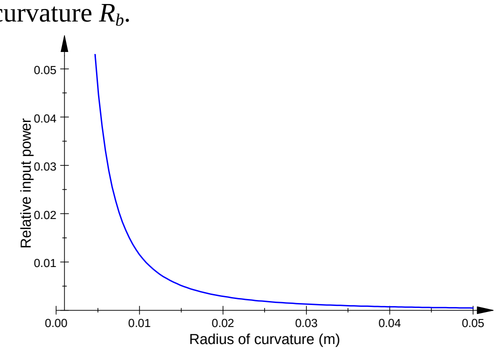

Fig. 16 Relative input power vs. radius of curvature

The numerical simulation performed using COMSOL Multiphysics is aiming to obtain an insight on the laser intensity distribution across the transverse section of the optic fiber. The option **2D** was used for the **Space Dimension**. Then the **RF Module** -> **Perpendicular Waves** -> **Hybrid-Mode Waves** -> **Mode analysis** options was used. The geometry of the transverse optical fiber cross section was developed considering realistic parameters. Elliptical deformation of the optical fiber was considered in order to resemble the bend.

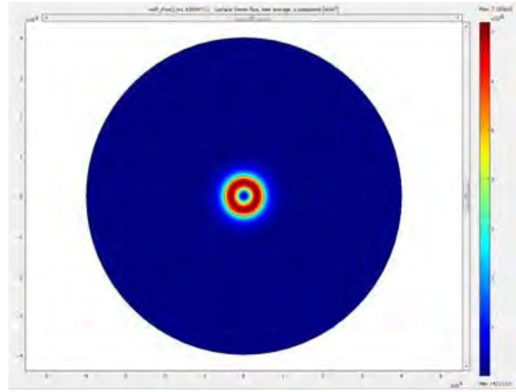

Fig. 17 The numerical simulated time averaged laser power flow across the transverse section of a single mode optical fiber with a core of 10 µm diameter and a cladding of an overall 80 µm diameter.

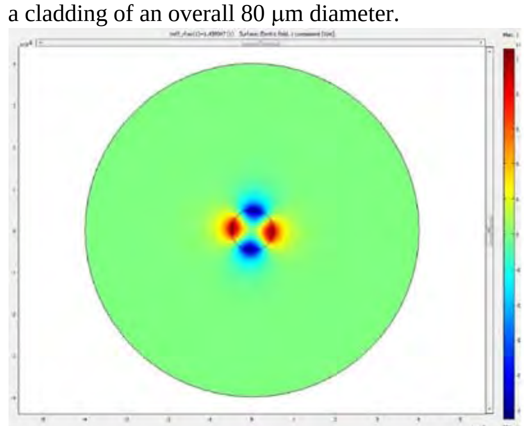

Fig. 18 The numerical simulated time averaged laser electric field distribution into the transverse section of a singlemode optical fiber with a core of 10 µm diameter and a cladding of an overall 80 µm diameter

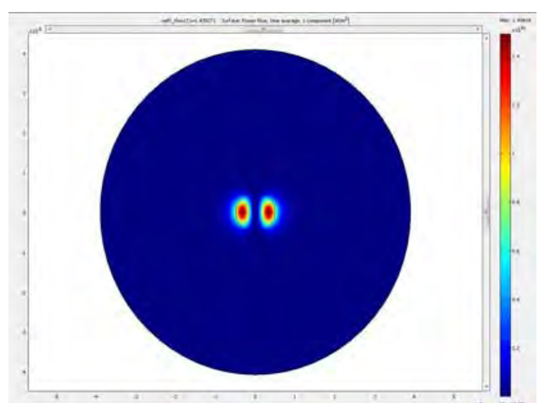

Fig. 19 The numerical simulated time averaged laser power flow across the transverse section of a single mode optical fiber with a core of 8.82 µm, 11.33 µm axes and a cladding of 70.59 µm, 90.67 µm axes.

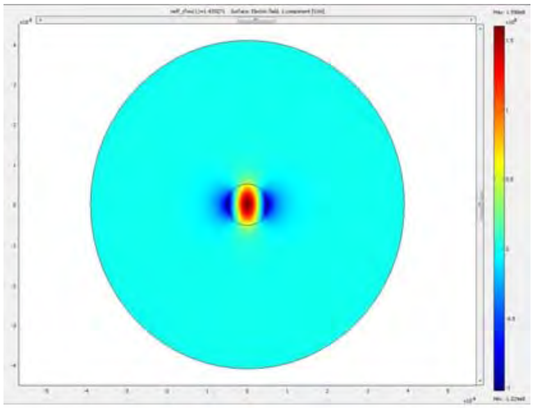

Fig. 20 The numerical simulated time averaged laser electric field distribution into the transverse section of a singlemode optical fiber with a core of 8.82 μm and 11.33 μm axes and a cladding of 70.59 μm and 90.67 μm axes

The procedure tried during numerical simulation consists in considering the laser beam propagation along the bending such as the optical fiber appears as of an elliptical cross section.

7. Conclusions

In this paper we have demonstrated the versatility of COMSOL Multiphysics regarding the modeling and simulation of DFB-FL sensor bending deformation.

The obtained COMSOL Multiphysics models are under development for fulfillment of aeronautic industry design needs. The considered development includes comparison with experimental results.

8. References

1. J. Hubner, P. Varming, and M. Kristensen, "Five wavelength DFB fiber laser source for WDM systems," Electron. Lett., vol. 33, no. 2, pp.139–140 (1997)

2. M. Ibsen, S. U. Alam, M. N. Zervas, A. B. Grudinin, and D. N. Payne, "8-and 16-channel all-fiber DFB laser WDM transmitters with integrated pump redundancy," IEEE Photon. Technol. Lett., vol. 11, no. 9, pp. 1114–1116 (Sep. 1999)

3. H. N. Poulsen, P. Varming, A. Buxens, A. T. Clausen, P. Munoz, P. Jeppesen, C. V. Poulsen, J. E. Pedersen, and L. Eskildsen, "1607 nm DFB fiber laser for optical communcation in the L-band," presented at the Eur. Conf. Optical Communications (ECOC), Nice, France, Sep. 26–30, Paper MoB2.1 (1999).

4. L. B. Fu, R. Selvas, M. Ibsen, J. K. Sahu, J. N. Jang, S. U. Alam, J. Nilsson, D. J. Richardson, D. N. Payne, C. Codemard, S. Goncharov, I. Zalevsky, and A. B. Grudinin, "Fiber-DFB laser array pumped with a single 1-W CW Yb-Fiber Laser," IEEE Photon. Technol. Lett., vol. 15, no. 5, pp. 655–657 (May 2003)

5. Z. E. Haratjunian, W. H. Loh, R. I. Laming, and D. N. Payne, "Single polarization twisted distributed feedback fiber laser," Electron. Lett., vol. 32, no. 4, pp. 346–348 (1996)

[6] H. Storoy, B. Sahlgren, and R. Stubbe, "Single polarization fiber DFB laser," Electron. Lett., vol. 33, no. 1, pp. 56–58 (1997)

[7] J. L. Philipsen, M. O. Berendt, P. Varming, V. C. Lauridsen, J. H. Povlsen, J. Hubner, M. Kristensen, and B. Palsdottir, "Polarization control of DFB fiber laser using UV-induced birefringent phase-shift," Electron. Lett., vol. 34, no. 7, pp. 678–679 (1998)

[8] J. T. Kringlebotn, W. H. Loh, and R. I. Laming, "Polarimetric Er3+- doped fiber distributed-feedback laser sensor for differential pressure and force measurements," Opt. Lett., vol. 21, no. 22, pp. 1869–1871 (1996)

[9] O. Hadeler, E. Ronnekleiv, M. Ibsen, and R. I. Laming, "Polarimetric fiber distributed feedback laser sensor for simultaneous strain and temperature measurements," Appl. Opt., vol. 38, no. 10, pp. 1953–1958 (1999)

[10] O. Hadeler, M. Ibsen, and M. N. Zervas, "Distributed-feedback fiber laser sensor for simultaneous strain and temperature measurements operating in the radio-frequency domain," Appl. Opt., vol. 40, no. 19, pp. 3169–3175 (2001)

[11] C. A. Codemard, L. Hickey, K. Yelen, D. B. S. Soh, R.Wixey,M. Coker, M. N. Zervas, and J. Nilsson, "400 mW 1060 nm ytterbium doped fiber DFB laser," presented at the Photonics West LASE, San Jose, CA, Paper 5335-11 (Jan.24 –29, 2004)

[12] H. Kogelnik and C. V. Shank, "Coupled-wave theory of distributed feedback lasers," J. Appl. Phys., vol. 43, no. 5, pp. 2327–2335 (1972)

[13]J. T. Kringlebotn, J. L. Archambault, L. Reekie, and D. N. Payne, "Er3+ Yb3+ codoped fiber distributed-feedback laser," Opt. Lett., vol. 19, no.24, pp. 2101–2103 (1994)

[14] V. C. Lauridsen, J. H. Povlsen, and P. Varming, "Design of DFB fiber lasers," Electron. Lett., vol. 34, no. 21, pp. 2028–2030 (1998)

[15] V. C. Lauridsen, J. H. Povlsen, and P. Varming,"Optimising erbium-doped DFB fiber laser length with respect to maximum output power," Electron. Lett., vol. 35, no. 4, pp. 300–302 (1999)

[16] M. Ibsen, E. Ronnekleiv, G. J. Cowle, M. O. Berendt, O. Hadeler, M. N. Zervas, and R. Laming, "Robust high power (>20 mW) all-fiber DFB lasers with unidirectional and truly single polarization outputs,"presented at the Conf. Lasers and Electro-Optics (CLEO), Baltimore, MD, Paper CWE4 (May 1999).

[17] K. Yelen, L. M. B. Hickey, and M. N. Zervas, "A new design approach for fiber DFB lasers with improved efficiency," IEEE J. Quantum Electron., vol. 40, no. 6, pp. 711–720 (June 2004)

[18] W. W. Rigrod, "Saturation effects in high-gain lasers," J. Appl. Phys., vol. 36, no. 8, pp. 2487–2490 (1965)

[19] G. Morthier and R. Baets, "Design of index-coupled DFB lasers with reduced longitudinal spatial hole burning," J. Lightw. Technol,, vol. 9, no. 10, pp. 1305–1313 (Oct. 1991)

20. Snyder A W and Love J D, Optical Waveguide Theory, Kluwer Academic Publishers, (2000)

21. Snyder A W and Love J D Reflection at a curved dielectric interface electromagnetic tunnelling IEEE Trans Microwave Theory Tech 23, 134 – 141

22. Besley J A and Love J D, Supermode analysis of fibre transmission Proc IEEE 144, 411 – 419, (1997)